Electron Spin Resonance of Nd^{3+} Pairs in $LaCl_3$ and $LaBr_3$†

K. L. BROWER AND H. J. STAPLETON*
Department of Physics and Materials Research Laboratory, University of Illinois, Urbana, Illinois
AND
E. O. BROWER
Department of Computer Science, University of Illinois, Urbana, Illinois
(Received 10 January 1966)

We have examined the electron-spin-resonance spectra due to Nd^{3+} pairs in $LaCl_3$ and $LaBr_3$. These measurements were made at 4.2°K and 9 kMc/sec using 0.1–2.0 at.% doping of enriched even-even isotopes of neodymium. A general anisotropic exchange interaction between two real spins is transformed into an effective-spin Hamiltonian formalism containing a Zeeman term and a traceless coupling tensor A_{ij} between two effective spins each of magnitude $\frac{1}{2}$. This latter term represents an anisotropic effective spin interaction within the triplet levels of the system. About 5000 resonances due to allowed and forbidden transitions within these triplet levels were observed and fitted to this Hamiltonian for various angles θ, between the magnetic field **H** and the crystal axis, and ϕ, between **H** and the plane containing a second-neighbor pair. Some resonances due to first-neighbor pairs were shifted by 2500 Oe from the unpaired-ion resonance and require analysis techniques other than perturbation theory. The observed symmetry of the second-neighbor interaction tensors in these two salts suggests that the halide ions play an important role. By removing the dipolar contributions to A_{ij}, quantitative results regarding the nature of the nondipolar spin-spin interaction are obtained. No resonances attributable to pairs were detected in $LaCl_3$ doped with either Ce^{3+} or Er^{3+}.

I. INTRODUCTION

AN examination of the usual electron spin resonance (ESR) line due to even-even isotopes of trivalent neodymium in single crystals of anhydrous lanthanum trichloride reveals an angularly dependent, unresolved satellite structure. These splittings are observed in crystals containing a few percent Nd^{3+} substituted for La^{3+} and indicate a symmetry which is lower than the axial symmetry surrounding the positive ion site. The concentration dependence of the relative intensities of the satellites to the main ESR line suggests a Nd-Nd pair interaction. Eisenstein, Hudson, and Mangum[1] have studied the magnetic susceptibility of concentrated neodymium trichloride and (99% Nd, 1% La) Cl_3 and interpret their results in terms of a strong superexchange interaction between the Nd^{3+} ions via Cl^- ions coupled with a much weaker dipole-dipole interaction. In this paper we report our measurements on the spin-resonance spectrum of Nd-Nd pairs in lightly doped single crystals of $LaCl_3$ and $LaBr_3$. We have analyzed our data in terms of a spin Hamiltonian which includes an anisotropic interaction between two effective spins of magnitude $\frac{1}{2}$. We shall refer to this interaction as a spin-spin interaction.

We have analyzed in detail those ESR spectra which we believe to be due to nearest-neighbor and next-nearest-neighbor Nd pairs in $LaCl_3$ and $LaBr_3$. These pair interactions produce satellites which are removed from the usual ESR line of an isolated Nd^{3+} ion by as much as 2500 Oe. The previously mentioned unresolved structure appearing on the usual ESR line is apparently due to much weaker spin-spin interactions between very distant neodymium pairs.

A brief resumé of the experimental apparatus and procedure is contained in Sec. II. Section III describes how the Zeeman and Nd-Nd pair interactions can be formulated in terms of a spin Hamiltonian, and the validity of perturbation theory is discussed. Section IV contains the analysis of our data for first and second nearest-neighbor interactions between even-even isotopes of Nd^{3+} in $LaCl_3$ and $LaBr_3$. Section V contains a discussion and interpretation of these results.

II. EXPERIMENTAL PROCEDURE

The pair spectra due to first and second nearest-neighbor Nd^{3+} pairs in these salts were observed with a standard ESR X-band reflection spectrometer employing crystal detection. The samples were mounted on a vertical rotatable end wall of a cylindrical cavity which resonated in a TE_{111} mode around 9 kMc/sec. The hexagonal symmetry axis of each sample was adjusted to lie in the horizontal plane and the vertical microwave field H_1 was always perpendicular to the horizontal dc magnetic field **H**. The spectra at liquid-helium temperatures were displayed on a strip-chart recorder for various values of θ, the angle between **H** and the crystalline axis. Generally θ was varied in 1° steps from $\theta=0°$ to $\theta=90°$. Magnetic-field measurements were made with a rotating-coil gaussmeter[2] to an accuracy of ±2 Oe at intervals of 100–200 Oe. The neodymium concentrations studied were nominally 0.1–2.0 at. % and generally consisted of enriched isotopic mixtures containing 97.7%

† Supported in part by the Advanced Research Projects Agency under Contract SD-131 and in part by the Alfred P. Sloan Foundation.
* Alfred P. Sloan Research Fellow.
[1] J. C. Eisenstein, R. P. Hudson, and B. W. Mangum, Phys. Rev. 137, A1886 (1965).
[2] George Associates, Model 203, Berkeley, California.

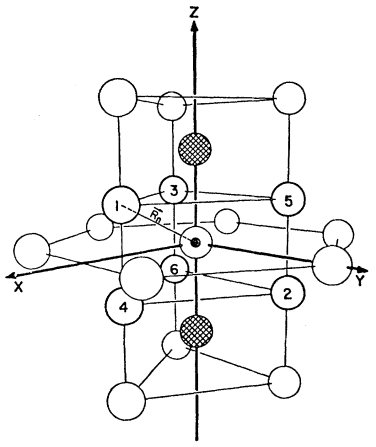

FIG. 1. Arrangement of the rare-earth cations in $LaCl_3$ and $LaBr_3$. The shaded ions on the Z axis represent the two nearest neighbors of the central ion at the origin of our coordinate system. The next-nearest neighbors are labeled from 1 to 6 and correspond to the numbering convention used in the text. The positions of the halide ions have been omitted from the figure.

even-even isotopes. The samples were cylindrical, 4 mm o.d.×6 mm long, and were prepared by a composite of standard techniques.[3,4]

III. THEORY

The appropriate spin Hamiltonian for isolated, even-even isotopes of Nd^{3+} in $LaCl_3$ is[3]

$$\mathcal{H}=g_{\parallel}\beta H_z S_z+g_{\perp}\beta(H_x S_x+H_y S_y), \quad (1)$$

where $g_{\parallel}=3.996\pm0.001$, $g_{\perp}=1.763\pm0.001$, and $S=\frac{1}{2}$. Since the closest excited crystal-field states are about 115.4 cm^{-1} above the ground doublet for Nd^{3+} in $LaCl_3$,[5] the effect of excited state admixtures should be negligible and an i-j pair interaction should be expressible in a spin Hamiltonian which is bilinear in the effective spins $\mathbf{S}^i=\mathbf{S}^j=\frac{1}{2}$. Transforming the magnetic dipole-dipole interaction into this form is straight forward and Baker[6] has illustrated the transformation of an isotropic exchange interaction between two real spins $\mathfrak{S}^i$ and $\mathfrak{S}^j$ into an anisotropic interaction between the corresponding effective spins $\mathbf{S}^i$ and $\mathbf{S}^j$. In this special case the anisotropy arises from the axial symmetry of the $\mathbf{g}$ tensor which enters through the relation $\mathfrak{S}^i=(\Lambda-1)\mathbf{g}\cdot\mathbf{S}^i/\Lambda$ where Λ is the Landé factor of the free-ion ground level. An anisotropic exchange interaction between two real spins will be of the form $\mathfrak{S}^i\cdot\mathfrak{J}\cdot\mathfrak{S}^j$ where $\mathfrak{J}$ is a symmetric second rank tensor. When this interaction is transformed into fictitious spin, it will appear as $\mathbf{S}^i\cdot\mathbf{K}'\cdot\mathbf{S}^j$ where

$$\mathbf{K}'=\left(\frac{\Lambda-1}{\Lambda}\right)^2\mathbf{g}\cdot\mathfrak{J}\cdot\mathbf{g}, \quad (2)$$

and $\mathbf{g}$ is a diagonal tensor with elements $g_{\perp}$, $g_{\perp}$, and $g_{\parallel}$ If we now write the total spin-spin interaction, including the dipole-dipole contribution, as $\mathbf{S}^i\cdot\mathbf{K}\cdot\mathbf{S}^j$ and incorporate it in a Zeeman spin Hamiltonian, the resulting system is most easily analyzed in terms of singlet and triplet states. Since ESR transitions are only observed between the triplet states, it is useful to rewrite the interaction as a sum of isotropic and traceless anisotropic interactions[7]:

$$\mathbf{S}^i\cdot\mathbf{K}\cdot\mathbf{S}^j=J\mathbf{S}^i\cdot\mathbf{S}^j+\mathbf{S}^i\cdot\mathbf{A}\cdot\mathbf{S}^j, \quad (3)$$

where Trace $\mathbf{A}=0$ and $3J=$Trace $\mathbf{K}$. The isotropic interaction produces a splitting of magnitude J between the singlet state and the center of gravity of the triplet states. The anisotropic term produces splittings within the triplet levels without altering their center of gravity. The isotropic term can be dropped from our ESR spin Hamiltonian since singlet-triplet transitions are forbidden and its only effect will be as an additive constant. The resulting form is

$$\mathcal{H}=\beta\mathbf{H}\cdot\mathbf{g}\cdot(\mathbf{S}^i+\mathbf{S}^j)+\mathbf{S}^i\cdot\mathbf{A}\cdot\mathbf{S}^j, \quad (4)$$

where $S^i=\frac{1}{2}$, $S^j=\frac{1}{2}$, but $S^i+S^j=1$ only, and Trace $\mathbf{A}=0$.

The symmetry of the La^{3+} sublattice in $LaCl_3$ or $LaBr_3$ is D_{3h}. Figure 1 illustrates[8] the location of the first- and second-nearest-neighbor cations and defines a set of crystal axes X, Y, Z in which $\mathbf{g}$, $\mathbf{H}$, and $\mathbf{A}$ will be defined. There are 2 first-neighbor sites lying a distance of ±4.366 Å along the threefold symmetry axis in $LaCl_3$.[9] This separation is 4.501 Å in $LaBr_3$.[9] The 6 second-neighbor sites are located at a distance of 4.83 and 5.11 Å in $LaCl_3$ and $LaBr_3$, respectively. The crystal Z axis is parallel to the threefold rotational axis. For any particular second-neighbor pair, the direction of the X axis is such that the vector $\mathbf{R}_n$ joining that particular pair is in the $++$ quadrant of the XZ plane. Rather than specifying the orientation of $\mathbf{H}$ relative to the 6 inequivalent second-neighbor coordinate systems, we shall specify the 6 corresponding orientations of $\mathbf{H}$ relative to one particular second-neighbor pair and its (X,Y,Z) coordinate system in which $\mathbf{g}$ and $\mathbf{A}$ are expressed. Thus, for second neighbors

$$\mathbf{H}=H(\sin\theta\cos\phi_n,\ \sin\theta\sin\phi_n,\ \cos\theta), \quad (5)$$

where

$$\phi_n=\phi_1+(n-1)60^\circ \quad n=1, 2, \cdots 6 \quad (6)$$

and the numbering convention of Fig. 1 is followed.

[3] C. A. Hutchison, Jr., and E. Y. Wong, J. Chem. Phys. **29**, 754 (1958).
[4] D. M. Gruen, J. C. Conway, and R. D. McLaughlin, J. Chem. Phys. **25**, 1102 (1956). In addition we received helpful information in the form of private communications with C. A. Hutchison, Jr., B. W. Mangum, and M. Abraham.
[5] J. C. Eisenstein, J. Chem. Phys. **39**, 2134 (1963).
[6] J. M. Baker, Phys. Rev. **136**, A1341 (1964).
[7] J. H. E. Griffiths, J. Owen, J. G. Park, and M. F. Partridge, Proc. Roy. Soc. (London) **A250**, 84 (1959).
[8] Perspective-view routine programmed by H. F. Jordan for Cal Comp digital plotter.
[9] W. A. Zachariasen, Acta Cryst. **1**, 265 (1948).

The matrix elements of our spin Hamiltonian are most simply calculated in a different coordinate system x, y, z, where z is parallel to the strong field spin precession axis[10] and y is parallel to the vertical component of the oscillating microwave magnetic field. The advantage of this approach over that of quantizing $\mathbf{S}$ along the crystalline c axis is that the coefficients of the various spin operators in Eq. (4) contain all the angular dependence and the matrix elements of $\mathcal{H}$ are calculated between triplet basis states having the form:

$$\begin{aligned}|S=1, S_z\rangle &= |S^i, S_z{}^i; S^j, S_z{}^j\rangle,\\ |1,1\rangle &= |\tfrac{1}{2},\tfrac{1}{2};\tfrac{1}{2},\tfrac{1}{2}\rangle,\\ |1,0\rangle &= (|\tfrac{1}{2},\tfrac{1}{2};\tfrac{1}{2},-\tfrac{1}{2}\rangle+|\tfrac{1}{2},-\tfrac{1}{2};\tfrac{1}{2},\tfrac{1}{2}\rangle)/\sqrt{2},\\ |1-1\rangle &= |\tfrac{1}{2},-\tfrac{1}{2};\tfrac{1}{2},-\tfrac{1}{2}\rangle\end{aligned} \tag{7}$$

The spin Hamiltonian in this x, y, z coordinate system becomes $\mathcal{H}=\mathcal{H}_0+\mathcal{H}'$ where

$$\begin{aligned}\mathcal{H}_0 &= g\beta H(S_z{}^i+S_z{}^j)+\alpha S_z{}^i S_z{}^j,\\ \mathcal{H}' &= \eta S_x{}^i S_x{}^j+\gamma S_y{}^i S_y{}^j+\delta(S_x{}^i S_y{}^j+S_y{}^i S_x{}^j)\\ &\quad +\xi(S_x{}^i S_z{}^j+S_z{}^i S_x{}^j)+\zeta(S_y{}^i S_z{}^j+S_z{}^i S_y{}^j),\\ \alpha &= A_{11}p^2(v^2-u^2)+A_{33}(q^2-p^2u^2)+2A_{13}pqv\\ &\quad +2A_{12}p^2\,uv+2A_{23}pqu,\\ \eta &= A_{11}q^2(v^2-u^2)+A_{33}(p^2-q^2u^2)-2A_{13}pqv\\ &\quad +2A_{12}q^2uv-2A_{23}pqu,\\ \gamma &= A_{11}(u^2-v^2)-A_{33}v^2-2A_{12}uv,\\ \delta &= -2A_{11}quv-A_{33}quv+A_{13}pu\\ &\quad +A_{12}q(v^2-u^2)-A_{23}pv,\\ \xi &= A_{11}pq(v^2-u^2)-A_{33}pq(1+u^2)+A_{13}(q^2-p^2)v\\ &\quad +2A_{12}pquv+A_{23}(q^2-p^2)u,\\ \zeta &= -2A_{11}puv-A_{33}puv-A_{13}qu\\ &\quad +A_{12}p(v^2-u^2)+A_{23}qv,\\ p &= g_\perp\sin\theta/g,\\ q &= g_{\parallel}\cos\theta/g,\\ u &= \sin\phi_n,\\ v &= \cos\phi_n,\\ g &= \{g_{\parallel}{}^2\cos^2\theta+g_\perp{}^2\sin^2\theta\}^{1/2}.\end{aligned} \tag{8}$$

Because of the relative strengths of the spin-spin and Zeeman interactions for nearest neighbors, a perturbation calculation of the magnetic-field intensities at resonance completely breaks down at frequencies around 9 kMc/sec. A perturbation approach is valid for the weaker second-neighbor interactions.

Restricting ourselves to second-neighbor interactions, the energy levels of the triplet states can be calculated from Eq. (8) using third-order perturbation theory in $\mathcal{H}'$.[11] The allowed transitions within the triplet states correspond to transitions in which $S=1$, $\Delta S=0$, $\Delta S_z=\pm1$ in the high-field limit and give rise to resonances with magnetic-field values above and below the value observed for unpaired ions. The field values calculated from third-order perturbation theory are:

$$\begin{aligned}&H(\sigma,\nu,\theta,\phi_n,\mathbf{g},\mathbf{A})\\ &=\frac{1}{g\beta}\Big[\epsilon-\Psi+\Omega-\frac{\Gamma}{\Delta+\Psi}+\frac{\Gamma}{2(\Delta-\Psi)}-\frac{\Upsilon}{2\Delta}-\frac{\Omega\Gamma}{(\Delta+\Psi)^2}\\ &\quad -\frac{\Omega\Gamma}{2(\Delta-\Psi)^2}+\frac{\Phi}{4\Delta(\Delta+\Psi)}+\frac{\Phi}{2(\Delta+\Psi)(\Delta-\Psi)}\Big],\end{aligned} \tag{9}$$

where

$$\begin{aligned}\Gamma &= (\tfrac{1}{4})(\xi^2+\zeta^2),\\ \Upsilon &= (\tfrac{1}{16})(\eta-\gamma)^2+(\tfrac{1}{4})\delta^2,\\ \Phi &= \sigma[(\tfrac{1}{8})(\eta-\gamma)(\xi^2-\zeta^2)+(\tfrac{1}{2})\delta\xi\zeta],\\ \Psi &= \sigma\alpha/2,\\ \Omega &= (\sigma/4)(\eta+\gamma),\\ \epsilon &= h\nu,\end{aligned} \tag{10}$$

and

$$\Delta=g\beta H_{\rm exp}\approx\tfrac{1}{2}\{\epsilon-\Psi+\Omega+[(\epsilon-\Psi+\Omega)^2-2(\Gamma+\Upsilon)]^{1/2}\}.$$

Here $H_{\rm exp}$ is the observed field position of the resonance line and σ is a parameter of unit magnitude with a sign such that σA_{33} is negative for the high-field satellite at $\theta=0°$ and positive for the low-field satellite at $\theta=0°$.

The "forbidden" transition, corresponding to $S=1$, $\Delta S=0$, $\Delta S_z=\pm2$ in the high-field limit, occurs at a field value of

$$\begin{aligned}&H_f(\sigma=1,\nu,\theta,\phi_n,\mathbf{g},\mathbf{A})\\ &=\frac{1}{2g\beta}\Big[\epsilon-\frac{2\Gamma\Delta^2+\Phi\Psi}{2\Delta(\Delta^2-\Psi^2)}-\frac{\Upsilon}{\Delta}+\frac{2\Omega\Gamma\Delta\Psi}{(\Delta^2-\Psi^2)^2}\Big],\end{aligned} \tag{11}$$

where the symbols are defined in Eq. (10) except the value of Δ is now given by

$$\Delta=g\beta H_{\rm exp}\approx\frac{\epsilon+\{\epsilon^2-8(\Gamma+\Upsilon)\}^{1/2}}{4}. \tag{12}$$

Equation (9), which gives the value of $H(\sigma,\nu,\theta,\phi_n,\mathbf{g},\mathbf{A})$, has certain symmetry properties which are useful in data analysis. The field H is invariant under the following operations:

$$\begin{aligned}H(\sigma,\mathbf{A}) &= H(-\sigma,-\mathbf{A}),\\ H(\phi,A_{13},A_{23}) &= H(\phi+180°,-A_{13},-A_{23}),\\ H(\phi,\mp g_{\parallel},\pm g_\perp) &= H(\phi+180°,\pm g_{\parallel},\mp g_\perp),\\ H(\mathbf{g}) &= H(-\mathbf{g}),\\ H(\theta=90°,\phi) &= H(\theta=90°,\phi+180°).\end{aligned} \tag{13}$$

[10] B. Bleaney, Phil. Mag. **42**, 441 (1951).

[11] L. D. Landau and E. M. Lifschitz, *Quantum Mechanics, Non-relativistic Theory* (Addison-Wesley Publishing Company, Inc., Reading, Massachusetts, 1958), Vol. 3, Chap. 6, p. 136.

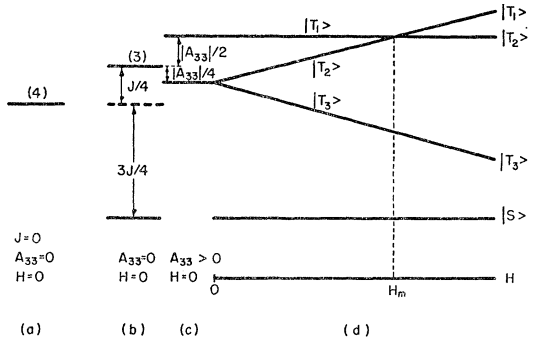

FIG. 2. Schematic energy-level diagram for Nd^{3+} pairs in $LaCl_3$ or $LaBr_3$ for various interactions: (a) fourfold degeneracy of two effective spins of $\frac{1}{2}$ each in the absence of a magnetic field or a spin-spin interaction; (b) isotropic spin-spin interaction producing singlet $|S\rangle$ and triplet $|T_i\rangle$ levels; (c) splitting of the triplet levels due to the further addition of an axially symmetric but traceless anisotropic spin-spin interaction; (d) additional splitting of the levels due to an external magnetic field directed along the symmetry axis. H_m is the field value at which levels $|T_1\rangle$ and $|T_2\rangle$ become degenerate under these conditions.

Furthermore, the approximate values of H near $\theta=0°$ and $\theta=90°$ are

$$H(\sigma,\nu,\theta\ll 1,\phi,\mathbf{g},\mathbf{A}) \approx\frac{1}{g\beta}\left[\epsilon-\frac{3\sigma}{2}(\tfrac{1}{2}A_{33}+A_{13}\theta v+A_{23}\theta u)\right] \quad (14)$$

and

$$H\left(\sigma,\nu,\theta\approx\frac{\pi}{2},\phi,\mathbf{g},\mathbf{A}\right) \approx\frac{1}{g\beta}\left\{\epsilon+\frac{3\sigma}{4}[A_{11}(u^2-v^2)+A_{33}u^2-2A_{12}\,uv]\right\} \quad (15)$$

We turn now to the case of nearest-neighbor interactions where perturbation theory breaks down for X-band microwave frequencies. We must therefore diagonalize $\mathcal{H}$ exactly, which is equivalent to finding the roots of the secular equation

$$\lambda^3-b_1\lambda-b_0=0, \quad (16)$$

where the coefficient of the λ^2 term vanishes because the Trace $\mathbf{A}=0$ and

$$b_1=\Delta^2+\Psi^2/4-\Psi\Omega+\Upsilon+\Gamma,$$

$$b_0=\frac{\Delta^2\Psi}{2}-\Delta^2\Omega-\frac{\Psi^3}{8}+\frac{\Psi^2\Omega}{4}-\frac{\Phi}{2}+\frac{\Upsilon\Psi}{2}-\Upsilon\Omega-\frac{\Gamma\Psi}{2}, \quad (17)$$

$$\sigma\equiv+1.$$

The properties of these roots are the same as the properties of H given in Eq. (13).

IV. ANALYSIS

From our magnetic-resonance data we wish to determine the elements of the $\mathbf{g}$ and $\mathbf{A}$ tensors which occur in the Hamiltonian of Eq. (4) and which are associated with the first- and second-neighbor Nd^{3+} pairs in $LaCl_3$ and $LaBr_3$. A least-squares fitting program (LSFP) was written specifically for both types of neighbor pairs and provisions were made which allowed any or all of the data for a particular crystal and neighbor to be included in the fit. The convergence properties of these programs were excellent and all computations were performed on the University of Illinois Illiac II.

A. First-Neighbor Interactions

Theoretically, the symmetry of the local environment around a nearest-neighbor pair is axial, and this was verified experimentally. Therefore, only three quantities $g_{\parallel}$, $g_{\perp}$, and A_{33} should be required to fit the data since $A_{11}=A_{22}=-A_{33}/2$. Furthermore, as shown in Fig. 2, the zero-field splitting of the triplet for this symmetry is $3|A_{33}|/4$. Our convention for labeling the triplet eigenstates $|T_i\rangle$, $i=1, 2, 3$, is such that

$$|T_i\rangle=\sum_{j=1}^{3} C_{ij}|S=1, S_z=2-j\rangle, \quad (18)$$

$$\langle T_k|\mathcal{H}|T_l\rangle=E_k\delta_{kl},$$

and

$$E_1\geq E_2\geq E_3.$$

For an orientation of the external field $\mathbf{H}$ parallel to the symmetry axis, the eigenstates are simply the basis states, and they split according to the schematic diagram of Fig. 2. At a field value labeled H_m in Fig. 2, $|T_1\rangle$ and $|T_2\rangle$ become degenerate at $\theta=0°$ and according to our labeling convention, the wave function $|T_1\rangle$ and $|T_2\rangle$ must be interchanged. For fields $H<H_m$, $|T_1\rangle=|S=1, S_z=0\rangle$, $|T_2\rangle=|S=1, S_z=1\rangle$, and $|T_3\rangle=|S=1, S_z=-1\rangle$. It is apparent from Fig. 2 that if $h\nu<3|A_{33}|/4$ for $\theta=0°$, the only allowed transitions are between $|T_1\rangle$ and $|T_2\rangle$ and that these will occur at two different fields above and below H_m. If, on the other hand, $h\nu>3|A_{33}|/4$ transitions between $|T_1\rangle$ and $|T_3\rangle$ are allowed as well as between $|T_1\rangle$ and $|T_2\rangle$.

Samples of neodymium-doped $LaBr_3$ exhibited two ESR lines at $\theta=0°$ which we attribute to first-neighbor pairs. When the microwave frequency was lowered by about 0.4 kMc/sec, the magnetic field positions of the

TABLE I. Best fitting elements of the axially symmetric $\mathbf{g}$ and $\mathbf{A}$ tensors for the ESR of nearest-neighbor Nd^{3+} pairs in (98% La, 2% Nd) Br_3 at 4.2°K and 9.050 kMc/sec. The fit is between the exact energy levels of the interaction Hamiltonian given by Eq. (4) of the text and the energy of the microwave quantum. Only the relative signs of the $\mathbf{A}$ tensor are known and the values listed here assume a negative value of A_{33}. Ninety-five resonances are fitted by these parameters with an rms deviation in wave number of 0.0006 cm^{-1}.

i,j	A_{ij} (cm^{-1})	ΔA_{ij} (cm^{-1})	$\lvert g_{ij}\rvert$	Δg_{ij}
1, 1=2, 2	0.2874	±0.0001	1.843	±0.001
3, 3	−0.5748	±0.0001	3.924	±0.002

two resonances were each displaced toward one another by approximately 60 Oe. This implies that we are observing transitions only between $|T_1\rangle$ and $|T_2\rangle$. For all angles θ between 0° and 90°, the energy difference ΔE between states $|T_1\rangle$ and $|T_2\rangle$ is obtained from the appropriate roots of Eq. (16) and is of the form

$$\Delta E(\theta,\mathbf{g},\mathbf{A},H)=2b_1^{1/2}|\sin(\mu/3)|\,, \tag{19}$$

where

$$\cos\mu=(3/b_1)^{3/2}(b_0/2)\,. \tag{20}$$

Both the high- and low-field ESR lines corresponding to transitions between $|T_1\rangle$ and $|T_2\rangle$ were fitted to Eq. (19) by minimizing $\sum_i(h\nu-\Delta E_i)^2$ with respect to A_{33} in a least-squares sense and with respect to $g_{\parallel}$ and $g_{\perp}$ by a direct search minimization procedure. The results of such a calculation are summarized in Table I for 95 data points. None of the signs of the quantities could be determined on the basis of the magnetic-field values and further attempts using signal strengths were inconclusive. In Fig. 3 the theoretical and experimental field positions of the nearest-neighbor ESR lines in $LaBr_3$ are plotted as a function of θ, in terms of ΔH, where

$$\Delta H=H-h\nu/g\beta \tag{21}$$

and g is calculated from the values of $g_{\parallel}$ and $g_{\perp}$ for the pair. In this figure the loop corresponds to transitions between $|T_1\rangle$ and $|T_2\rangle$ while the other curve represents

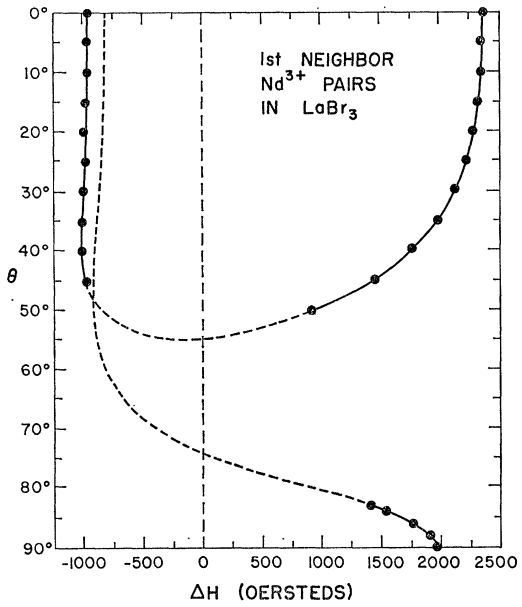

FIG. 3. Theoretical fit of the observed ESR field positions for the nearest-neighbor Nd^{3+} pairs in $LaBr_3$ at 9.050 kMc/sec and 4.2°K. The curves are plotted as a function of θ, the angle between the magnetic field and the crystalline symmetry axis, and ΔH, as defined in Eq. (21) of the text. The solid lines are theoretical fits in regions where resonances are observed while the dotted curves are extrapolated values using the same parameters, which are listed in Table I. In the notation of Fig. 2, the loop corresponds to transitions between $|T_1\rangle$ and $|T_2\rangle$ while the other curve represents transitions between $|T_2\rangle$ and $|T_3\rangle$. Only $\frac{1}{4}$ of the observed data are shown on the solid curves.

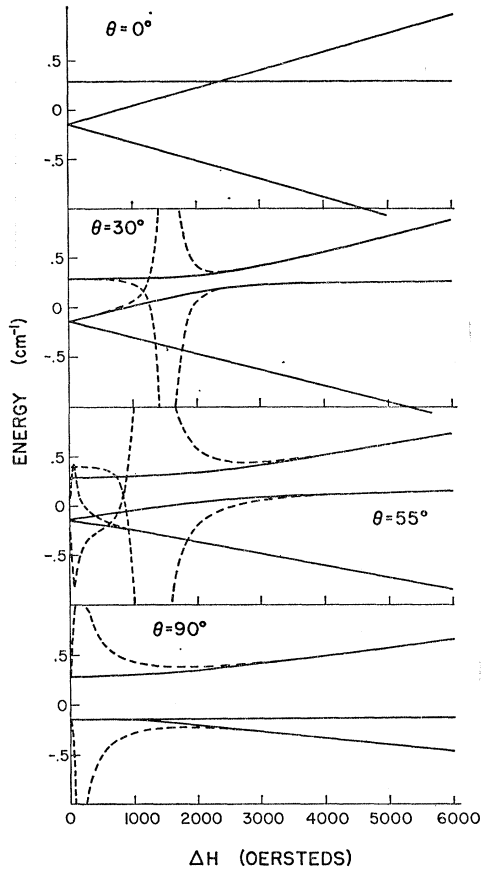

FIG. 4. Triplet energy levels of Nd^{3+} pairs in $LaBr_3$ as a function of magnetic field for various angles θ. The solid curves represent exact solutions to the Hamiltonian of Eq. (4) using the data of Table I while the dashed curves are the erroneous results of a third-order perturbation theory.

transitions between $|T_2\rangle$ and $|T_3\rangle$. The solid portion of the curves contains typical data points and represents those regions over which the ESR pair spectra were observed. These resonance lines displayed a typical peak-to-peak derivative linewidth of 15 Oe. The dotted portion corresponds to regions where transitions are energetically possible but were not observed because of such factors as: low-transition probabilities, large linewidths, or interference with stronger resonances from other sources.

Using the data of Table I, the energy levels can be computed for various values of θ, and the results are shown in Fig. 4. The solid lines correspond to the roots of Eq. (16) while the dotted curves represent the erroneous results of a third-order perturbation calculation.

Figure 5 shows the results of measurements on $LaCl_3$ doped with Nd^{3+}. The solid lines with typical data points represent regions where first-neighbor ESR lines could be identified. These lines had a peak-to-peak derivative linewidth of about 12 Oe. Since the low-field transition at $\theta=0°$ and $\nu=9.050$ kMc/sec was not observed, it was not initially possible to assign uniquely

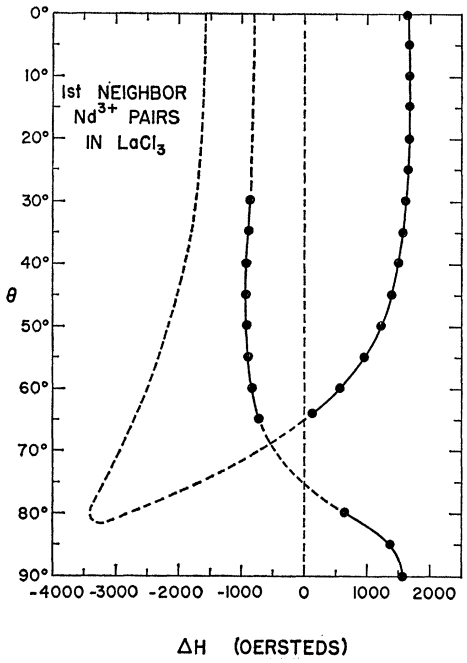

FIG. 5. Theoretical fit of the observed ESR field positions for nearest-neighbor Nd^{3+} pairs in $LaCl_3$ at 9.031 kMc/sec and 4.2°K. The figure is plotted in the same manner as Fig. 3 except that the theoretical fit was made using only the high-field lines for $\theta \leq 64°$, and the fitting parameters are listed in Table II. We indicate here only $\frac{1}{4}$ of the observed data.

the transition involved for the observed lines. Thus, only the 64 data points corresponding to the high-field transition ($|T_1\rangle$ to $|T_2\rangle$) between $0° \leq \theta \leq 64°$ were used in the LSFP. From the excellent fit of the remaining points in Fig. 5, it is clear that they correspond to transitions between $|T_2\rangle$ and $|T_3\rangle$. Furthermore at lower frequencies ($\nu = 8.399$ kMc/sec) the low-field resonance was observed for $0° \leq \theta \leq 35°$ at fields around 150 Oe. The results of the first- neighbor data in $LaCl_3$ are summarized in Table II.

Finally, a word about mixing coefficients and transition probabilities seems in order. Figure 6 contains plots of the quantities $|C_{ij}|^2$ which appear in Eq. (18) as mixing coefficients of the three basis states. They are plotted here as a function of magnetic field for a fixed value of θ at 55° using the $LaBr_3$ data of Table I. The

TABLE II. Best fitting elements of the axially symmetric **g** and **A** tensors for the ESR of the nearest-neighbor Nd^{3+} pairs in (98% La, 2% Nd) Cl_3 at 4.2°K and 9.031 kMc/sec. The fit is between the exact energy levels of the interaction Hamiltonian given by Eq. (4) of the text and the energy of the microwave quantum. Only the relative signs of the **A** tensor are known and the values listed here assume a negative value of A_{33}. Sixty-four resonances are fitted by these parameters with an rms deviation in wave numbers of 0.0003 cm^{-1}.

i, j	A_{ij} (cm^{-1})	ΔA_{ij} (cm^{-1})	$\lvert g_{ij}\rvert$	Δg_{ij}
1, 1=2, 2	0.2082	±0.0001	1.710	±0.002
3, 3	−0.4164	±0.0001	4.018	±0.004

TABLE III. Best fitting elements of the symmetric **A** tensor for the ESR of next-nearest-neighbor Nd^{3+} pairs in (98% La, 2% Nd) Cl_3 at 4.2°K and 9.038 kMc/sec. The fit is between the observed and calculated values of the magnetic field at resonance. One thousand thirty-six resonances are fitted with an rms deviation of 8.6 Oe using $\phi_1 = 1.9° \pm 2.2°$, $|g_{\|}| = 4.001 \pm 0.002$, $|g_{\perp}| = 1.768 \pm 0.001$, and the values of A_{ij} listed below. The signs of the elements are relative to an assumed positive value of A_{33}. $\Delta A_{ij}^{\text{exp}}$ is the error assuming that ϕ_1 is known exactly, ΔA_{ij}^{ϕ} is the error due entirely to the uncertainty in ϕ_1, and ΔA_{ij} is the resultant total error.

	$LaCl_3$	Second neighbor	$\phi_1 = 1.9° \pm 2.2°$	
i, j	A_{ij} (cm^{-1})	$\Delta A_{ij}^{\text{exp}}$ (cm^{-1})	ΔA_{ij}^{ϕ} (cm^{-1})	ΔA_{ij} (cm^{-1})
1, 1	−0.1035	±0.0001	±0.0001	±0.00015
2, 2	−0.06713	±0.00014	±0.0001	±0.00017
3, 3	+0.1706	±0.0001	±0.0000	±0.0001
1, 2	+0.00136	±0.00011	±0.0013	±0.0013
1, 3	±0.03866	±0.00010	±0.00005	±0.00011
2, 3	±0.00146	±0.00010	±0.0015	±0.0015

transition probability between eigenstates $|T_i\rangle$ and $|T_j\rangle$ is proportional to $|\langle T_i|S_y|T_j\rangle|^2$ where $S_y = S_y{}^i + S_y{}^j$ since the states are quantized in the xyz coordinate system where the microwave magnetic field is parallel to the y axis which is always perpendicular to the plane containing the crystal symmetry axis and the static magnetic field. Figure 7 contains a plot of $|\langle T_i|S_y|T_j\rangle|^2$ as a function of H for $\theta = 55°$ using the data of Table I.

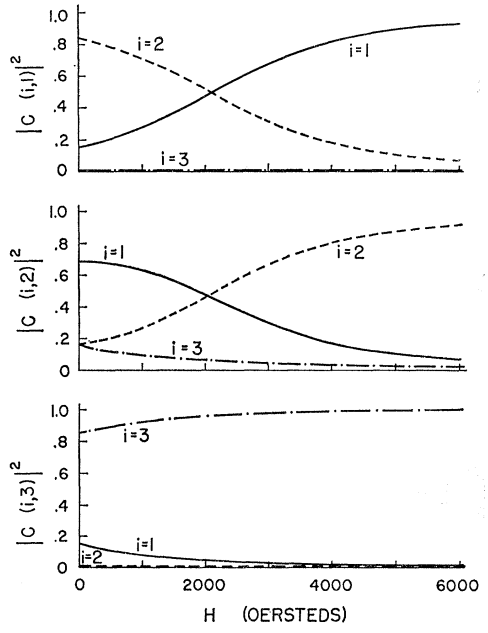

FIG. 6. The field dependence of the square of the mixing coefficients C_{ij} for nearest-neighbor Nd^{3+} pairs in $LaBr_3$ at $\theta = 55°$ based on the data of Table I. These coefficients appear in Eq. (18) of the text and describe the eigenfunctions as admixtures of the triplet state basis functions having an axis of quantization along the strong-field-precession axis described in Ref. 10. The j subscript takes on values 1, 2, or 3 corresponding to $S=1, S_z=1$, 0, −1, respectively, while the i subscript refers to the eigenfunctions $|T_i\rangle$.

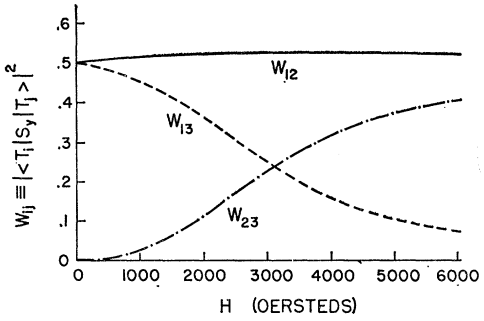

FIG. 7. Magnetic-field dependence of the relative transition probability W_{ij} among the triplet levels of nearest-neighbor Nd^{3+} pairs in $LaBr_3$ at $\theta=55°$. The microwave magnetic field is taken perpendicular to a plane containing the static magnetic field and the crystalline axis. These calculations are based on the data of Table I and Fig. 6.

B. Second-Neighbor Interactions

The analysis of second-neighbor interactions is more complicated than for first neighbor because of the breakdown of axial symmetry. We shall make the simplifying assumption that the **g** tensor remains axially symmetric, and later we shall present some justification for this. Since the **A** tensor is always given in the XYZ coordinate system of Fig. 1, which by definition contains a second-neighbor pair in the ++ quadrant of the XZ plane, one might hope that this plane would be one of reflection symmetry for the interaction with the result that $A_{23}=A_{12}=0$. Unfortunately a good fit of the data is not possible under this constraint. This suggests that the previously neglected Cl^- ions, which lie near the Nd^{3+} ions and which do not possess reflection symmetry in the XZ plane, are important in the interaction. This would seem to support the superexchange model of Eisenstein *et al.*[1]

If the interaction did possess reflection symmetry in the XZ plane, one could determine the principal azimuthal coordinate ϕ_1 in the following manner. To a given set of data one assigns a fixed but completely arbitrary azimuthal angle ϕ_1'. Since this assignment would not generally be correct, the resulting values of A_{12} and A_{23} would not be zero. One could then rotate the **A** tensor about the Z axis through an angle of magnitude $\tilde{\alpha}$ such that A_{12} and A_{23} were simultaneously zero, thus determining the correct value of the principal azimuthal coordinate to be $\phi_1=\phi_1'+\tilde{\alpha}$.

However reflection symmetry in the XZ plane does not exist, so we have adopted the procedure outlined below for the determination of ϕ_1. We first assign a fixed but arbitrary azimuthal angle ϕ_1' to each set of data and then determine the rotation angles $\tilde{\alpha}_1$ and $\tilde{\alpha}_2$ about the Z axis which make A_{23} and A_{12} vanish respectively. We then take $\phi_1=\phi_1'+(\tilde{\alpha}_1+\tilde{\alpha}_2)/2$ as the best estimate and define its error as $\Delta\phi=|\tilde{\alpha}_1-\tilde{\alpha}_2|/2$. If the XZ plane were one of reflection symmetry for this interaction, $\Delta\phi$ would be zero. It is noteworthy that one cannot determine ϕ_1 by including it as a variable in the magnetic field LSFP since $\sum(H-H_{\text{exp}})^2$ is invariant with respect to ϕ_1. This is because we have assumed an axially symmetric **g** tensor and the **A** tensor possesses no symmetry properties.

In view of the uncertainty in ϕ_1, it is useful to introduce three different types of errors. If there were no uncertainty in ϕ_1, each element of $\mathbf{A}(XYZ)$ would still possess an error due to the usual random experimental errors, and we shall refer to this as the experimental error $\Delta A_{ij}^{\text{exp}}$. In addition there is an error in the elements of $\mathbf{A}(XYZ)$ due solely to the uncertainty in ϕ_1, and we denote it as ΔA_{ij}^{ϕ}. Finally, we define the total

TABLE IV. Best fitting elements of the symmetric **A** tensor for the ESR of next-nearest-neighbor Nd^{3+} pairs in (98%, La, 2% Nd) Cl_3 at 4.2°K and 9.031 kMc/sec. The results are presented in a manner similar to Table III except $\phi_1=32.0°\pm1.6°$. One thousand forty-two resonances are fitted with an rms deviation of 8.5 Oe.

	$LaCl_3$	Second neighbor	$\phi_1=32.0°\pm1.6°$	
i,j	A_{ij} (cm^{-1})	$\Delta A_{ij}^{\text{exp}}$ (cm^{-1})	ΔA_{ij}^{ϕ} (cm^{-1})	ΔA_{ij} (cm^{-1})
1, 1	−0.1033	±0.0001	±0.00005	±0.0001
2, 2	−0.06739	±0.00015	±0.00005	±0.00015
3, 3	+0.1707	±0.0001	±0.00000	±0.0001
1, 2	+0.00099	±0.0001	±0.0010	±0.0010
1, 3	±0.03561	±0.0001	±0.00003	±0.0001
2, 3	±0.00099	±0.0001	±0.0010	±0.0010

TABLE V. Best fitting elements of the symmetric **A** tensor for the ESR of next-nearest-neighbor Nd^{3+} pairs in (98% La, 2% Nd) Cl_3 at 4.2°K and 9.033 kMc/sec. The results are presented in a manner similar to Table III except $\phi_1=46.3°\pm0.7°$. Three hundred twenty-nine resonances are fitted with an rms deviation of 9.3 Oe.

	$LaCl_3$	Second neighbor	$\phi_1=46.3°\pm0.7°$	
i,j	A_{ij} (cm^{-1})	$\Delta A_{ij}^{\text{exp}}$ (cm^{-1})	ΔA_{ij}^{ϕ} (cm^{-1})	ΔA_{ij} (cm^{-1})
1, 1	−0.1037	±0.0002	±0.00003	±0.0002
2, 2	−0.06667	±0.00024	±0.00003	±0.00024
3, 3	+0.1704	±0.0002	±0.00000	±0.0002
1, 2	−0.00126	±0.00023	±0.00043	±0.00049
1, 3	±0.03805	±0.00014	±0.000005	±0.00014
2, 3	±0.00044	±0.00024	±0.00044	±0.00050

TABLE VI. Best fitting elements of the symmetric **A** tensor for the ESR of next-nearest-neighbor Nd^{3+} pairs in (98% La, 2% Nd) Br_3 at 4.2°K and 9.047 kMc/sec. The fit is between the observed and calculated values of the magnetic field at resonance. Nine hundred ninety-two resonances are fitted with an rms deviation of 14 Oe using $\phi_1=4.1°\pm25.6°$, $|g_{\parallel}|=3.856\pm0.002$, $|g_{\perp}|=1.910\pm0.001$, and the values of A_{ij} listed below. The signs and errors are given according to the convention established in Table III.

	$LaBr_3$	Second neighbor	$\phi_1=4.1°\pm25.6°$	
i,j	A_{ij} (cm^{-1})	$\Delta A_{ij}^{\text{exp}}$ (cm^{-1})	ΔA_{ij}^{ϕ} (cm^{-1})	ΔA_{ij} (cm^{-1})
1, 1	−0.1030	±0.0002	±0.017	±0.017
2, 2	−0.0650	±0.0002	±0.017	±0.017
3, 3	+0.1680	±0.0001	±0.0000	+0.0001
1, 2	+0.0220	±0.0002	±0.013	±0.013
1, 3	±0.0385	±0.0002	±0.007	±0.007
2, 3	±0.0176	±0.0002	±0.017	±0.017

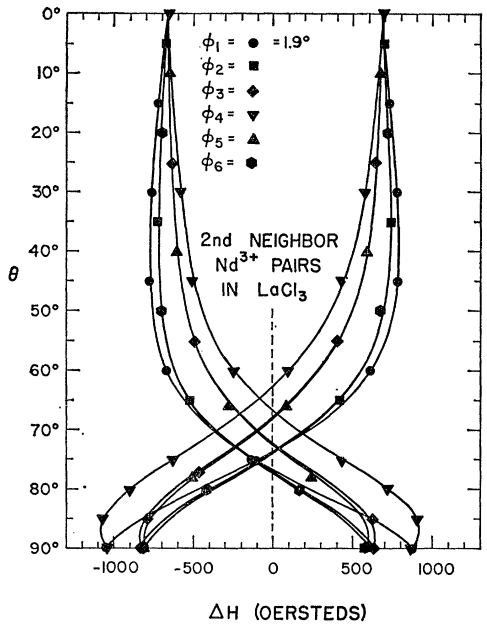

FIG. 8. Theoretical fit of the observed ESR field positions for next-nearest-neighbor Nd^{3+} pairs in $LaCl_3$ at 9.038 kMc/sec and 4.2°K. The curves are plotted in the same manner as Fig. 3 using the data of Table IX and $\phi_1=1.9°$. The characters corresponding to the six observed inequivalent values of ϕ_n are noted in the figure and the principal azimuthal coordinate ϕ_1 was determined to be 1.9° from the data of Table III. Only a fraction of the 1036 observed resonances are shown here.

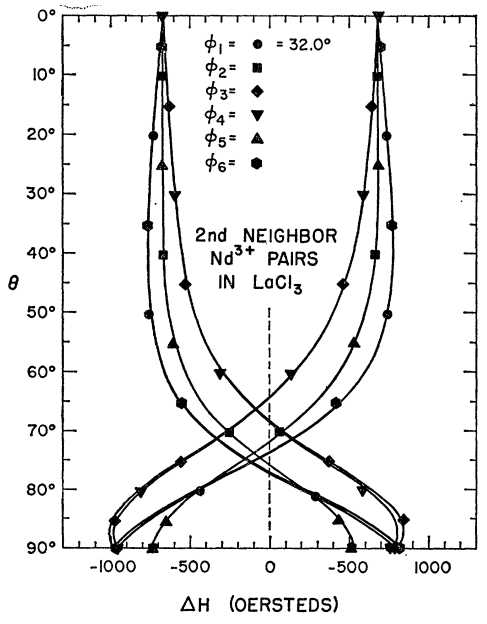

FIG. 9. Theoretical fit of the observed ESR field positions for next-nearest-neighbor Nd^{3+} pairs in $LaCl_3$ at 9.031 kMc/sec and 4.2°K. The curves are plotted in the same manner as Figs. 3 and 8 using the data of Table IX and $\phi_1=32.0°$. This principal value of the azimuthal coordinate was determined from the data of Table IV. Only 5% of the observed resonances are shown here.

TABLE VII. Best fitting elements of the symmetric A tensor for the ESR of next-nearest-neighbor Nd^{3+} pairs in (98% La, 2% Nd) Br_3 at 4.2°K and 9.051 kMc/sec. The results are presented in a manner similar to Table VI except $\phi_1=22.8°\pm24.0°$. One thousand fifteen resonances are fitted with an rms deviation of 12 Oe.

	$LaBr_3$	Second neighbor	$\phi_1=22.8°\pm24.0°$	
i,j	A_{ij} (cm^{-1})	ΔA_{ij}^{expt} (cm^{-1})	ΔA_{ij}^{ϕ} (cm^{-1})	ΔA_{ij} (cm^{-1})
1, 1	−0.1034	±0.0002	±0.016	±0.016
2, 2	−0.0649	±0.0002	±0.016	±0.016
3, 3	+0.1683	±0.0001	±0.0000	±0.0001
1, 2	+0.0215	±0.0002	±0.012	±0.012
1, 3	±0.0384	±0.0001	±0.007	±0.007
2, 3	±0.0171	±0.0001	±0.016	±0.016

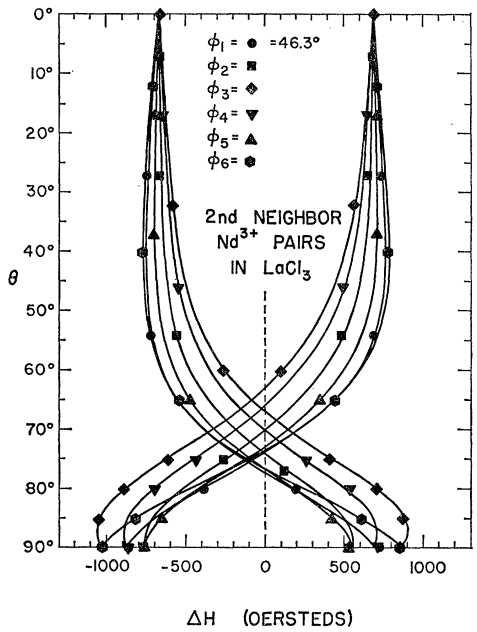

FIG. 10. Theoretical fit of the observed ESR field positions for next-nearest-neighbor Nd^{3+} pairs in $LaCl_3$ at 9.033 kMc/sec and 4.2°K. The curves are plotted in the same manner as Figs. 3 and 8 using the data of Table IX and $\phi_1=46.3°$. This value of the principal azimuthal coordinate was determined from the data of Table V. Only 20% of the observed resonances are shown here.

TABLE VIII. Best fitting elements of the symmetric A tensor for the ESR of next-nearest-neighbor Nd^{3+} pairs in (98% La, 2% Nd) Br_3 at 4.2°K and 9.042 kMc/sec. The results are presented in a manner similar to Table VI except $\phi_1=36.1°\pm24.7°$. Four hundred eighty-nine resonances are fitted with an rms deviation of 18 Oe.

	$LaBr_3$	Second neighbor	$\phi_1=36.1°\pm24.7°$	
i,j	A_{ij} (cm^{-1})	ΔA_{ij}^{expt} (cm^{-1})	ΔA_{ij}^{ϕ} (cm^{-1})	ΔA_{ij} (cm^{-1})
1, 1	−0.1029	±0.0003	±0.017	±0.017
2, 2	−0.0645	±0.0004	±0.017	±0.017
3, 3	+0.1674	±0.0003	±0.0000	±0.0003
1, 2	+0.0224	±0.0003	±0.015	±0.015
1, 3	±0.0385	±0.0003	±0.007	±0.007
2, 3	±0.0177	±0.0003	±0.017	±0.017

TABLE IX. Summary of the best fitting elements of the symmetric A tensor for the ESR of the next-nearest-neighbor Nd^{3+} pairs in (98% La, 2% Nd) Cl_3 at 4.2°K. The fitted data includes all the 2407 resonances observed at the three different values of ϕ_1 and ν listed in Tables III, IV, and V. The fit to the magnetic-field values has an rms deviation of 8.9 Oe. The signs and errors in the A tensor are listed according to the convention of Table III.

	$LaCl_3$		Second-neighbor summary	
	$\lvert g_{\parallel}\rvert = 4.001 \pm 0.002$,	$\Delta\phi = \pm 1.6°$,	$\lvert g_{\perp}\rvert = 1.768 \pm 0.001$	
i, j	A_{ij} (cm^{-1})	$\Delta A_{ij}^{\text{expt}}$ (cm^{-1})	ΔA_{ij}^{ϕ} (cm^{-1})	ΔA_{ij} (cm^{-1})
1, 1	−0.1033	±0.0002	±0.00006	±0.0002
2, 2	−0.0673	±0.0002	±0.00006	±0.0002
3, 3	+0.1706	±0.0002	±0.00000	±0.0002
1, 2	+0.0009	±0.0002	±0.001	±0.001
1, 3	±0.0387	±0.0001	±0.00003	±0.0001
2, 3	±0.0012	±0.0002	±0.0011	±0.0011

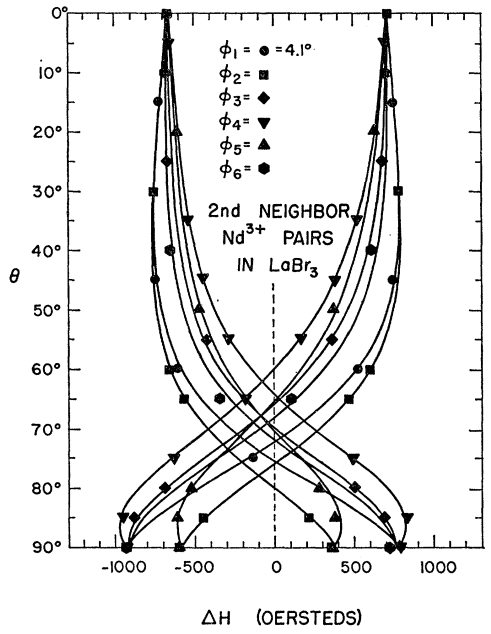

FIG. 11. Theoretical fit of the observed ESR field positions for next-nearest-neighbor Nd^{3+} pairs in $LaBr_3$ at 9.047 kMc/sec and 4.2°K. The curves are plotted in the same manner as Figs. 3 and 8 using the data of Table X and $\phi_1 = 4.1°$. This value of the principal azimuthal coordinate was determined from the data of Table VI. Only 6% of the observed resonances are shown here.

TABLE X. Summary of the best fitting elements of the symmetric A tensor for the ESR of the next-nearest-neighbor Nd^{3+} pairs in (98% La, 2% Nd) Br_3 at 4.2°K. The fitted data include all the 2496 resonances observed at the three different values of ϕ_1 and ν listed in Tables VI, VII, and VIII. The fit to the magnetic-field values has an rms deviation of 14.1 Oe. The signs and errors in the A tensor are listed according to the convention of Table III.

	$LaBr_3$		Second-neighbor summary	
	$\lvert g_{\parallel}\rvert = 3.856 \pm 0.002$,	$\Delta\phi = \pm 24.4°$,	$\lvert g_{\perp}\rvert = 1.910 \pm 0.001$	
i, j	A_{ij} (cm^{-1})	$\Delta A_{ij}^{\text{expt}}$ (cm^{-1})	ΔA_{ij}^{ϕ} (cm^{-1})	ΔA_{ij} (cm^{-1})
1, 1	−0.1032	±0.0001	±0.017	±0.017
2, 2	−0.0648	±0.0001	±0.017	±0.017
3, 3	+0.1680	±0.0001	±0.0000	±0.0001
1, 2	+0.0219	±0.0001	±0.014	±0.014
1, 3	±0.0384	±0.0001	±0.007	±0.007
2, 3	±0.0174	±0.0001	±0.016	±0.016

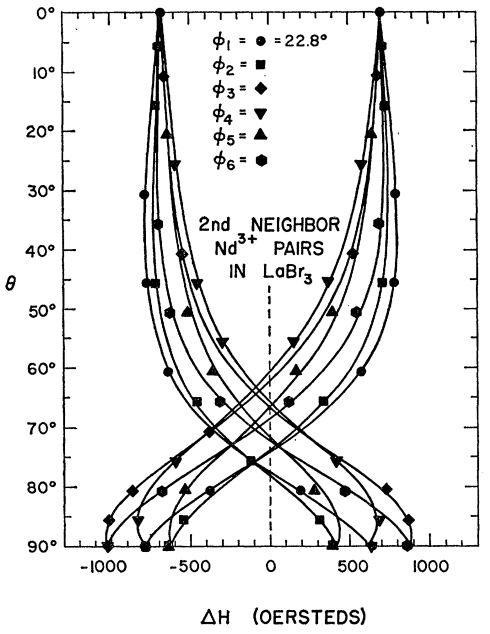

FIG. 12. Theoretical fit of the observed ESR field positions for next-nearest-neighbor Nd^{3+} pairs in $LaBr_3$ at 9.051 kMc/sec and 4.2°K. The curves are plotted in the same manner as Figs. 3 and 8 using the data of Table X and $\phi_1 = 22.8°$. This value of the principal azimuthal coordinate was determined from the data of Table VII. Only 7% of the observed data are shown here.

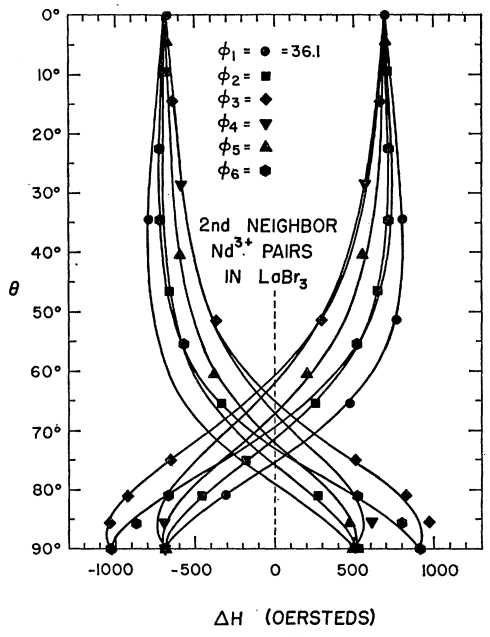

FIG. 13. Theoretical fit of the observed ESR field positions for next-nearest-neighbor Nd^{3+} pairs in $LaBr_3$ at 9.043 kMc/sec and 4.2°K. The curves are plotted in the same manner as Figs. 3 and 8 using the data of Table X and $\phi_1 = 36.1°$. This value of the principal azimuthal coordinate was determined from the data of Table VIII. Only 12% of the observed resonances are shown here.

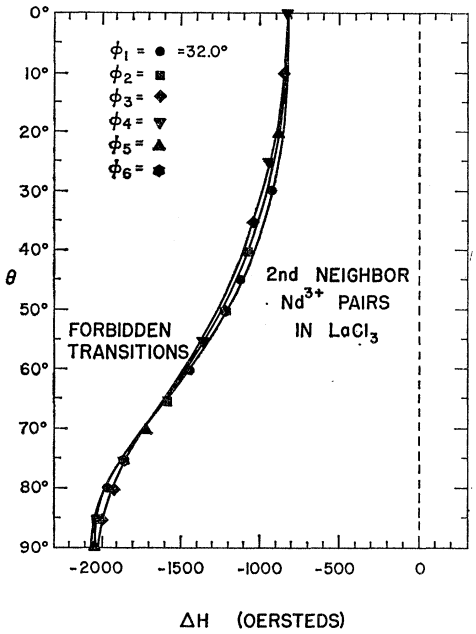

FIG. 14. Theoretical fit of the observed field positions of the six "forbidden" ESR lines for next-nearest-neighbor Nd^{3+} pairs in $LaCl_3$ at 9.031 kMc/sec and 4.2°K. The curves are plotted in the same manner as Figs. 3 and 8 using the data of Table IX and $\phi_1=32.0°$. This value of the principal azimuthal coordinate was determined from the data of Table IV. Only 4% of the observed resonances are shown here.

error ΔA_{ij} as the square root of the sum of the squares of $\Delta A_{ij}^{\text{exp}}$ and ΔA_{ij}^{ϕ}.

The values of $g_{\parallel}$, $g_{\perp}$, and A_{ij} (XYZ) which result from a fit of the 12-line allowed Nd^{3+} pair transitions in $LaCl_3$ and $LaBr_3$ to Eq. (9) for various values of ϕ_1 are listed in Tables III–VIII. Tables IX and X summarize the results of a single fit of all the chloride data and all the bromide data, respectively. Magnetic-field deviations are calculated from the data of these summary tables for each particular value of ν and ϕ_1 in Tables III–VIII, and the results are compared with experiments in Figs. 8–13. Typical peak-to-peak derivative linewidths for second-neighbor pairs in $LaCl_3$ and $LaBr_3$ are 5–10 and 7–15 Oe, respectively. The consistency of these data is noteworthy in view of the so-called error in ϕ_1. Finally, Fig. 14 illustrates the fit of the six "forbidden" transitions $(S=1, \Delta S_z=\pm 2)$ for second-neighbor Nd^{3+} pairs in $LaCl_3$ at 9.031 kMc/sec and $\phi_1=32°$ using the data of Table IX. The rms deviation between 500 observed and calculated field positions of the "forbidden" transitions in $LaCl_3$ based on the data of Table IX and $\phi_1=32°$ is 14.7 Oe. A similar rms deviation of the 266 observed and calculated forbidden transitions in $LaBr_3$ for $\phi_1=4.1°$ and 9.047 kMc/sec is 11.9 Oe.

V. DISCUSSION AND INTERPRETATION

We interpret the fact that A_{12} and A_{23} are nonzero for second-neighbor interactions as evidence that the pair coupling is not simply a direct Nd-Nd interaction since the XZ or 1, 3 plane contains all second-neighbor pairs by definition. The fact that there are two Cl^- ions in the neighborhood of each Nd second-neighbor pair and that these ions do not possess reflection symmetry in the 1, 3 plane tends to support the Cl^- assisted superexchange model of Eisenstein, Hudson, and Mangum.[1] Their differential susceptibility measurements on pure $NdCl_3$ exhibited field-dependent peaks around 1.745 and 1.035°K. They interpret the higher temperature as the onset of a ferromagnetic ordering of nearest neighbors and the lower temperature as the onset of an antiferromagnetic ordering between second neighbors. The whole interaction is sufficiently complex that it is difficult to make a reliable comparison between our tensor elements and their observed transition temperatures.

Nevertheless some quantitative features of the interaction can be determined. Table XI lists the contributions to the $\mathbf{A}$ tensor from first- and second-neighbor Nd dipole-dipole interactions in $LaCl_3$ and $LaBr_3$. Only the dipolar contribution to the element A_{13} has a sign dependence on $g_{\parallel}$ or $g_{\perp}$ in that its sign is proportional to the product $g_{\parallel}g_{\perp}$. If these values are compared with the corresponding elements listed in Tables I, II, IX, and X, it is noted that the dipolar contributions are roughly an order of magnitude smaller than the observed values except for A_{13} in the second-neighbor interactions. If for A_{13} we assume that the dipolar contribution is dominant, then the residual magnitude of that element is comparable to the magnitudes of A_{12} and A_{23} which have no dipolar origin and which are small compared to the diagonal terms. Therefore in our XYZ coordinate system, it is a good approximation to consider the nondipolar portion of the $\mathbf{A}$ tensor as diagonal.

In order to discuss what this implies about the real spin interaction $\mathfrak{S}^i \cdot \mathfrak{J} \cdot \mathfrak{S}^j$ through Eqs. (2) and (3), it is necessary to justify our use of an axially symmetric $\mathbf{g}$ tensor. It could be argued that the local symmetry around a Nd-Nd second-neighbor pair is lower than axial due to the existence of the pair and yet our data are well fit by the use of an axial $\mathbf{g}$ tensor. There is one minor discrepancy, however, if one examines the second-

TABLE XI. Summary of the dipole-dipole contributions to the interaction tensor A_{ij} for first- and second-neighbor pairs in $LaCl_3$ and $LaBr_3$. Only the sign of the A_{13} element for second-neighbor pairs is dependent upon the signs of $g_{\parallel}$ and $g_{\perp}$. Its sign is equal to the sign of the product $g_{\parallel}g_{\perp}$. The values listed here assume the magnitudes of $g_{\parallel}$ and $g_{\perp}$ which appear in Tables I, II, IX, and X.

Salt neighbor	$LaCl_3$ 1st	$LaBr_3$ 1st	$LaCl_3$ 2nd	$LaBr_3$ 2nd
A_{11} (cm^{-1})	0.0163	0.0173	−0.0167	−0.0168
A_{22}	0.0163	0.0173	0.0120	0.0118
A_{33}	−0.0326	−0.0346	0.0047	0.0050
A_{12}	...	...	...	...
A_{13}	...	...	±0.0329	±0.0283
A_{23}	...	...	...	...

neighbor pair spectra as a function of ϕ_1 at $\theta=90°$. At certain values of ϕ_1 our calculations indicate that the six high-field resonances should coalesce into a quartet and a doublet simultaneously with a similar pattern among the six low-field lines. What is experimentally observed is that both the high- and low-field patterns merge into a quartet and a doublet but not simultaneously in ϕ_1. The observed difference $\Delta\phi_1$ between the two events was never greater than 6.5°. In an attempt to account for this effect, we broke the axial symmetry of the $\mathbf{g}$ tensor by adding a small perturbation $\mathcal{H}'=\beta\mathbf{H}\cdot\mathbf{g}'\cdot(\mathbf{S}^i+\mathbf{S}^j)$ where $\mathbf{g}'$ is a symmetric tensor with small but nonzero g_{11}' and g_{13}' elements. The major effect of such a perturbation arises from a second-order cross term between it and the spin-spin interaction. The result is a predicted field dependence in the quartet-doublet field difference which leads to a large asymmetry in this field splitting for high- and low-field resonances. Since this was not observed experimentally, we conclude that an axially symmetric $\mathbf{g}$ tensor is justified, but we are unable to explain the origin of the $\Delta\phi_1$ discrepancy at $\theta=90°$.

The real spin interaction tensor $\mathfrak{J}$ can be decomposed into isotropic and traceless parts according to

$$\mathfrak{J}_{ij}=\mathfrak{J}\delta_{ij}+\mathfrak{A}_{ij}, \tag{22}$$

where δ_{ij} is the Kronecker delta and Trace $\mathfrak{A}=0$. From Eqs. (2), (3), and (22) it follows that

$$\begin{aligned}
J&=C(g_\perp^2\mathfrak{J}+D),\\
A_{12}&=Cg_\perp^2\mathfrak{A}_{12},\\
A_{13}&=Cg_\parallel g_\perp\mathfrak{A}_{13},\\
A_{23}&=Cg_\parallel g_\perp\mathfrak{A}_{23},\\
A_{11}&=C(g_\perp^2\mathfrak{A}_{11}-D),\\
A_{22}&=C(g_\perp^2\mathfrak{A}_{22}-D),\\
A_{33}&=C(g_\perp^2\mathfrak{A}_{33}+2D),
\end{aligned}$$

where

$$C=\left(\frac{\Lambda-1}{\Lambda}\right)^2,$$

and

$$D=\tfrac{1}{3}(g_\parallel^2-g_\perp^2)(\mathfrak{J}+\mathfrak{A}_{33}). \tag{23}$$

Therefore, in the XYZ coordinate frame $\mathfrak{A}_{12}\approx\mathfrak{A}_{13}\approx\mathfrak{A}_{23}\approx0$. If the diagonal elements of $\mathfrak{A}$ were zero then $\mathbf{A}$ would be axially symmetric even for second-neighbor interactions. If we assume that the isotropic part of $\mathfrak{J}_{ij}$ is dominant and if in agreement with Eisenstein *et al.*,[1] we take the second-neighbor interaction as antiferromagnetic then A_{33} should be positive for second-neighbor pairs. This is how it is listed in Tables IX and X. If the dipolar contributions are removed using the data in Table XI, the net values of the diagonal elements are $A_{11}=-0.0866$ cm^{-1}, $A_{22}=-0.0793$ cm^{-1}, and $A_{33}=0.1659$ cm^{-1} for $LaCl_3$ and $A_{11}=-0.0864$ cm^{-1}, $A_{22}=-0.0766$ cm^{-1}, and $A_{33}=0.1630$ cm^{-1} for $LaBr_3$. The deviation from axial symmetry is thus ±0.0037 cm^{-1} and ±0.0049 cm^{-1} in the trichloride and tribromide, respectively. This indicates that $\mathfrak{J}$ is probably an order of magnitude greater than the diagonal elements of $\mathfrak{A}$.

In conclusion several points are worth noting. We have made a rough measurement of $|A_{33}|$ for both third- and fourth-neighbor pairs in $LaCl_3$ and obtain a common value of 0.01 cm^{-1} whereas the dipolar contributions are 0.0032 and -0.0031 cm^{-1}, respectively. We have searched for pair spectra in $LaCl_3$ containing 1% Ce^{3+} or Er^{3+} and except for occasional structure on the isolated ion resonance, nothing attributable to well-resolved pair spectra was observed. Er^{3+} was specifically chosen because of its narrow (3.3 Oe) ESR line in the perpendicular direction.[12] The sample examined was doped with enriched (97.9% even-even) Er isotopes and a search was made at $\theta=90°$ from 100 to 3000 Oe at 9.140 kMc/sec at 1.67°K. The value of $g_\perp$ for this ion in $LaCl_3$ is 8.757.[3] Our spectrometer sensitivity was sufficient to observe the residual 0.003% Pr^{3+} impurity in the lanthanum as well as some erbium hyperfine structure due to residual odd isotopes. A cerium-doped crystal of $LaCl_3$ was examined around $\theta=0°$ in the temperature range between 4.2 and 1.62°K at 8.7 kMc/sec with no evidence of pair spectra. We are unable to explain these negative results except to note that some calculations by Eisenstein *et al.*[1] on the expected strength of the spin-spin interaction in pure $CeCl_3$ and $PrCl_3$ indicate that it should be smaller by an order of magnitude in these salts. Nevertheless we should still be sensitive to such a reduced interaction. The relaxation time of Nd in $LaCl_3$ at 4.2°K is quite slow because of the absence of an Orbach mechanism, but Ce^{3+} and Er^{3+} are practically as slow at 1.6°K[12] so that relaxation rates cannot be influential in determining the effect. It is interesting to note that the actinide analog of Nd^{3+}, $4f^3$, which is U^{3+}, $5f^3$, does exhibit pair resonances[13,14] in $LaCl_3$ so that the electronic configuration seems to be quite important. We have estimated the strength of the quadrupole interaction between first-neighbor Nd pairs in $LaCl_3$ and found that it is orders of magnitude too small to account for our observations.

ACKNOWLEDGMENTS

We wish to thank Dr. J. M. Baker, Dr. J. C. Eisenstein, Professor C. P. Slichter, and Professor P. B. Dorain for helpful discussions.

[12] R. C. Mikkelson and H. J. Stapleton, Phys. Rev. **140**, A1968 (1965).
[13] C. A. Hutchison, Jr., P. M. Llewellyn, E. Y. Wong, and P. Dorain, Phys. Rev. **102**, 292 (1956).
[14] P. B. Dorain (private communication).